Journal of Materials Chemistry A

Accepted Manuscript

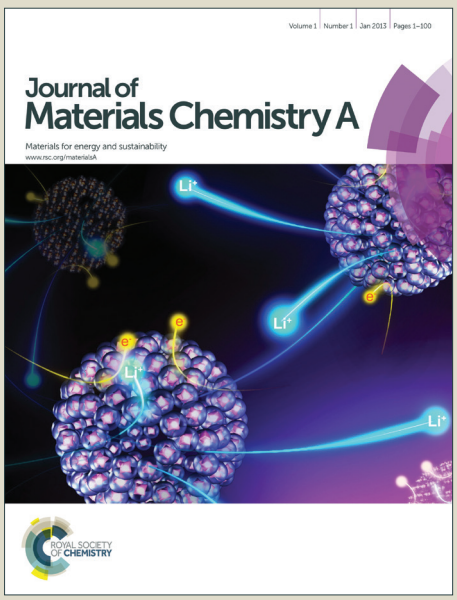

ROYAL SOCIETY OF CHEMISTRY

www.rsc.org/materialsA

Perovskite Processing for Photovoltaics: a Spectro-Thermal Evaluation

Alice E. Williams,[a] Peter J. Holliman,[b] Matthew J. Carnie,[a] Matthew L. Davies,[a] David A. Worsley,[a] Trystan M. Watson*[a]

[a] SPECIFIC, College of Engineering Swansea University, Baglan Bay Innovation and Knowledge Centre, Port Talbot, SA12 7AZ (UK)
[b] School of Chemistry, Bangor University, Bangor, Gwynedd, LL57 2UW (UK)

Abstract

Thermal analysis (TGA and DSC), coupled with evolved gas FTIR spectroscopy, have been used to study the changes occurring during, and differences between materials after, the annealing step of mixed-halide methylammonium lead halide perovskites. This is important because, to date, the material is the most efficient light harvester in highly efficient, 3rd generation perovskite photovoltaic devices, and processing plays a significant role in device performance. TGA-FTIR data show only solvent evolution during the annealing step, whilst post-annealing analysis shows that the resulting material still contains a significant amount of residual solvent; however, efficient DMF removal was possible using a silica gel desiccant for a period of 3 days. The data also show that methylammonium halide decomposition does not occur until temperatures well above those used for perovskite processing, suggesting that this is not a significant issue for device manufacture. The absence of a well-defined, reversible tetragonal – cubic phase change around 55 °C in the DSC data of the annealed material, and the presence of HCl in evolved gas analysed following thermal decomposition, demonstrates that $CH_3NH_3I_{3-X}Cl_X$ does retain some Cl after annealing and does not simply form stoichiometric $CH_3NH_3PbI_3$ as has been suggested by some workers.

1 Introduction

1.1 Perovskite as a Light Harvester

Snaith *et al.*'s report of using methylammonium lead halide ($CH_3NH_3PbX_3$) perovskites as the light-harvester in solid-state photovoltaic devices has led to substantial interest in this area.[1–8] These versatile materials, initially studied by Mitzi and coworkers,[9,10] were first used in photovoltaic applications in liquid-junction dye-sensitised solar cells.[1] More recently, and now more commonly, they have appeared in solid state devices with hole transport materials (HTM) instead of a liquid electrolyte.[3] The $CH_3NH_3PbX_3$ perovskite is generally deposited onto either a mesoporous metal oxide scaffold or a planar junction metal oxide, leading to devices with efficiencies in excess of 16 %. In dye-sensitized solar cells, an appropriate metal oxide such as TiO_2 is necessary to increase the surface area and light harvesting efficiency and to allow transport of the generated electrons, but perovskites can serve the dual function of light absorber and electron transporter, so do not necessarily require a mesoporous oxide layer.[2,3,5] Interestingly, as reported elsewhere, the perovskite is ambipolar in nature and can act as both electron and hole transporter, which has led to the production of working devices without the incorporation of an HTM layer[4]. Omission of these layers could lead to advantages such as reduction of energy losses, and increased J_{sc} and V_{OC}.[3,5]

A key step in manufacturing these devices is perovskite processing. This is commonly accomplished by spin-coating[3] or spray-depositing[11] a high concentration (40 wt. %) perovskite precursor solution on to the

substrate, followed by annealing at a temperature *ca*. 100 °C for up to 1 h.[3,12,13] It has been shown that deposition processes influence perovskite film coverage, morphology, structure and composition, which in turn play an important part in device efficiency; furthermore, the annealing temperature and duration have been reported to affect film thickness and coverage.[12–14] Since these processing conditions are highly influential on the final device characteristics, it is important to understand fully the effect of these factors on the resulting film.[6,12,13,15,16]

In a number of studies, a perovskite film cast from a precursor solution was air-dried for 30 min at room temperature in an inert atmosphere for 'slow solvent evaporation' prior to examining the effect of annealing on film coverage, although these workers did not present a direct comparison between materials that had been 'pre-dried' in this manner and 'freshly deposited'.[12,14] Other studies have investigated the effect of different annealing temperatures on optical absorption of the final film, and have shown that elevated temperature is required for good optical absorption, and consequently device performance;[13] however, to the best of our knowledge, no work has yet been carried out quantifying solvent loss from the perovskite material during annealing. It should be noted that for an analogous material, $CsSnI_3$, "polar organic solvent" (possibly DMF) loss was achieved at room temperature and solvent loss verified by FTIR,[17] but whether this was FTIR or TGA-FTIR was not specified.

Amongst other things, the annealing step is purported to remove volatile components that do not contribute, and may actually be detrimental, to the final structure and performance of the resulting material.[12–14] For example, when $CH_3NH_3PbI_{3-x}Cl_x$ films are deposited from $PbCl_2$ and CH_3NH_3I, chloride is reportedly absent from the resultant films.[13] These workers propose that, at T < 120 °C, CH_3NH_3Cl is produced alongside the final perovskite material and subsequently sublimes away as the perovskite (which they suggest is $CH_3NH_3PbI_3$) forms. They also propose that at higher temperatures (> 120 °C) decomposition to PbI_2, CH_3NH_3I and CH_3NH_3Cl occurs: although $CH_3NH_3PbI_3$ is reportedly stable up to 300 °C, the material has been seen to decompose at the significantly lower temperature of 140 °C.[13,18] It must be noted, however, that this was carried out under vacuum rather than atmospheric pressure,[18] and the precursor solution comprised PbI_2 and CH_3NH_3I rather than the mixed ($PbCl_2$/CH_3NH_3I) halide.[18]

There has been considerable thermal and spectroscopic work carried out to understand the structural changes of methylammonium lead halides and analogues containing different metal and organic cations,[19–21] and of the three methylammonium halides, CH_3NH_3I, CH_3NH_3Br and CH_3NH_3Cl.[22–29] This includes a recent publication by A. Dualeh *et al.*, in which a comprehensive study of the thermal properties of $CH_3NH_3PbX_3$ (X = I or Cl) and the relevant methylammonium halide precursors was undertaken;[30] however, a tandem calorimetric-spectroscopic study, whereby calorimetric events are directly correlated with evolved gases, has not been performed for these particular materials (although it has for quaternary alkylammonium halides).[31,32]

Hence, this paper describes a detailed study of the role of annealing in the loss of organic material from organolead perovskites by means of evolved gas analysis. Given their importance in these processes, the methylammonium halide salts CH_3NH_3Cl and CH_3NH_3I are also considered. Alternative methods of solvent removal have also been studied, *e.g.* slow, low-temperature solvent 'pre-drying' under N_2, as performed by Eperon *et al.*,[12,14] and low-temperature solvent evaporation in air conjunction with a desiccant. A full understanding of all these processes is crucial for their control and acceleration which, ultimately, is essential for scaling technology.

2. Experimental

2.1. Perovskite synthesis

All chemicals were obtained from Sigma-Aldrich and used without further purification unless otherwise stated. Methylammonium halides were prepared by reacting an excess of methylamine solution (33 wt. % in absolute ethanol) and the relevant acid halide (HI: 99.95 % purity, distilled, stabilised hydroiodic acid, 57 wt. % in H_2O; HCl: hydrochloric acid 37 % in H_2O) in ethanol; the reaction was carried out overnight under N_2. CH_3NH_3I was synthesised at room temperature and CH_3NH_3Cl in an ice bath. Ethanol was removed by vacuum rotary evaporation at 60 °C and the white crystals washed thoroughly in diethyl ether before overnight drying *in vacuo* at 60 °C. Perovskite precursor solutions were prepared to be 40 wt. % in anhydrous DMF. For $CH_3NH_3PbI_{3-x}Cl_x$, the samples were prepared using 3:1 (m/m) CH_3NH_3I : $PbCl_2$ and the reaction occurred at room temperature, agitating until all solids dissolved; for $CH_3NH_3PbI_3$ the samples were prepared using 1:1 (m/m) CH_3NH_3I : PbI_2 and the reaction was carried out stirring under reflux at 60 °C, ≥ 6 h. Solutions were filtered with a 20 μm Minisart filter (Fisher) before use. The typical XRD pattern for $CH_3NH_3PbI_3$ prepared under similar conditions is given in ESI Fig. 1.

2.2. Instrumental analysis

All equipment was obtained from Perkin Elmer unless otherwise stated. Thermogravimetric analyses (TGA) and differential scanning calorimetry (DSC) were carried out using a Pyris 1 TGA and a DSC 4000 respectively. All thermal analyses were carried out in open, disposable Al pans under dry N_2 (BOC) at 20 ml min^{-1}. For DSC, the sample was measured *w.r.t.* an identical reference pan. For each measurement, fresh perovskite precursor solution (10 – 20 μl, *ca.* 10 – 20 μg) was pipetted into a new pan to cover the base. Isothermal and temperature-ramp measurements were performed over a different temperature ranges and rates. Simultaneous thermal analysis - Fourier Transform infrared spectroscopy (STA-FTIR) was carried out on a STA 6000 coupled with a Frontier FTIR spectrometer using a TL 8000 transfer line held at 300 °C with a gas flow of 80 ml min^{-1}. The experiments were performed at atmospheric pressure under N_2 flow. Samples were placed into a ceramic crucible equipped with a thin, disposable Al liner. The furnace and ceramic crucible were cleaned as necessary using DMF followed by heating to 900 °C in air.

3. Results and Discussion

3.1. Thermal chemistry of $CH_3NH_3PbI_{3-x}Cl_x$ and $CH_3NH_3PbI_3$ in DMF

The rate of mass loss was measured for 40 wt. % DMF solutions of $CH_3NH_3PbI_{3-x}Cl_x$ (where $0 \leq x \leq 1$) and $CH_3NH_3PbI_3$ under isothermal conditions to mimic roll-to-roll processing, which could be used to manufacture perovskite PV devices. Solutions were heated from ambient to 100 °C in 1 min and the mass loss recorded over the following 15 min (Fig. 1a, main). This was repeated at different annealing temperatures from 30 – 100 °C until a steady mass was achieved and the maximum rate loss at each temperature was calculated (Fig. 1b).

The data in Figure 1a show that solvent loss for $CH_3NH_3PbI_{3-x}Cl_x$ is complete after 10 min, when a consistent mass of 40 % is achieved. The mass loss for the $CH_3NH_3PbI_3$ (Fig. 1a, red curves) exhibits a slightly different but repeatable profile with a more rapid mass loss up to *ca.* 7 min followed by an abrupt change to a

continued mass loss at a much reduced rate, which extends beyond the 16 min shown. In line with these data, the rate of maximum mass loss for both materials is similar up to 70 °C, but after this becomes more rapid for $CH_3NH_3PbI_3$ (circles) than for $CH_3NH_3PbI_{3-x}Cl_x$ (crosses). Assuming that complete solvent is required for optimal device performance, the $CH_3NH_3PbI_{3-x}Cl_x$ reaches a constant mass faster than the $CH_3NH_3PbI_3$, which appears to retains solvent (presumably as solvent of crystallisation) even after 15 min annealing at 110 °C. This could indicate differences in crystal structure that might lead to slower solvent diffusion through the structure of, and/or a greater solvent affinity for, $CH_3NH_3PbI_3$ than $CH_3NH_3PbI_{3-x}Cl_x$.

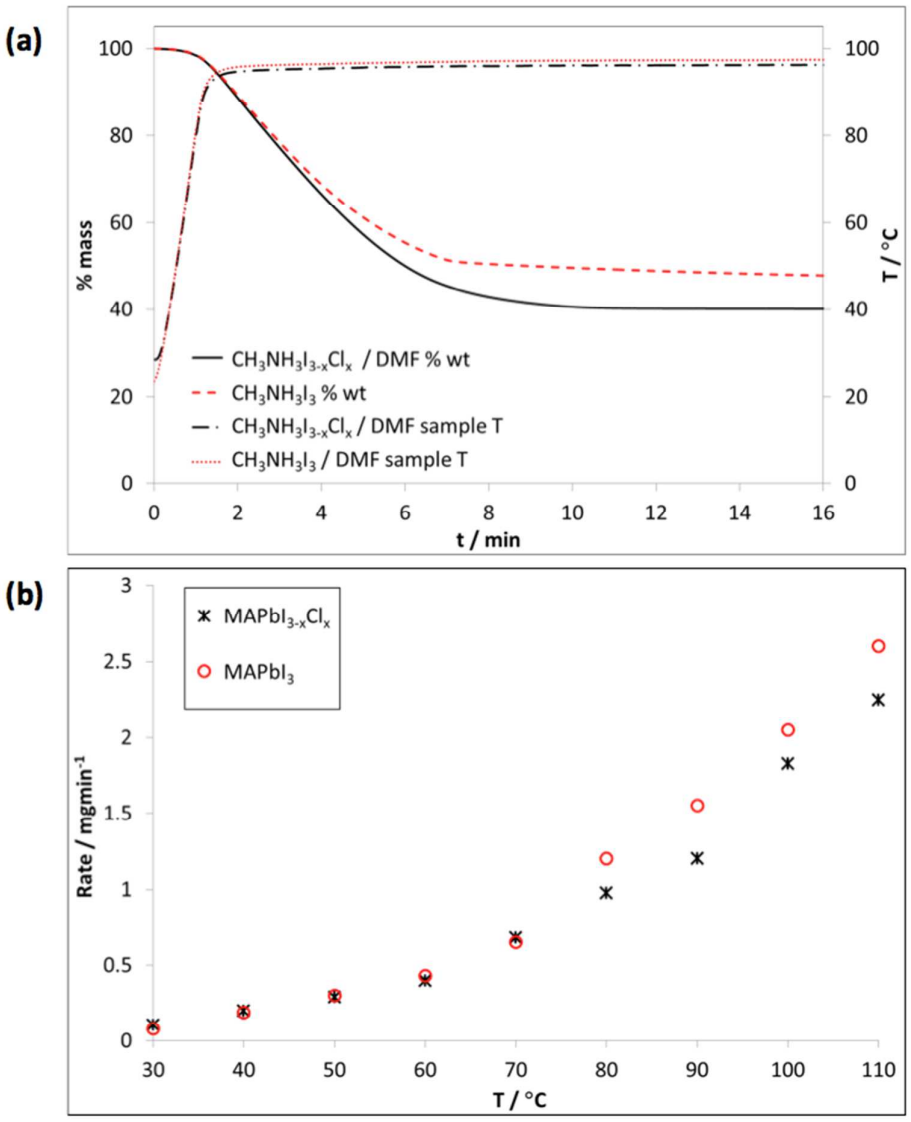

Figure 1: (a) Isothermal TGA of 40 wt. % DMF solutions of $CH_3NH_3PbI_{3-x}Cl_x$ (black solid line) and $CH_3NH_3PbI_3$ (red solid line) at *ca.* 100 °C following 1 min ramp; (b) maximum rate of mass loss of 40 wt. % DMF solutions of $CH_3NH_3PbI_{3-x}Cl_x$ (black crosses) and $CH_3NH_3PbI_3$ (red circles) *vs.* annealing temperature.

3.1. Thermal chemistry and evolved gas analysis

When considering what gives rise to the mass losses observed at these annealing temperatures (*i.e.* < 100

°C), the most likely candidates are the solvent, DMF (b.p. = 153 ± 1 °C)[33] and methylammonium halides CH_3NH_3I ($T_{sublimation}$ = 247 ± 26 °C)[30] and CH_3NH_3Cl ($T_{sublimation}$ = 195 ± 9 °C)[30], rather than PbI_2 (mp = 410 °C , bp = 872 °C (decomposes)).[34] Whilst the DMF might be expected to evaporate intact, the situation for the methylammonium halides is more complicated as they are salts. Whilst the thermodynamic and structural properties of methylammonium halides have been well-characterised, [22–30] the situation here is further complicated because perovskite deposition involves simultaneous solvation, chemical reaction, surface interaction, nucleation, precipitation and evaporation. Additionally, these processes occur within a heterogeneous, solvent-solid, diffusion-limited system, which is exposed to heat so the temperature rapidly ramps from ambient to the annealing temperature (100 °C) either in static or flowing gas, usually N_2 or air. To simplify the system, the thermal chemistry and tandem real-time gas sampling of the salts CH_3NH_3I and CH_3NH_3Cl has been studied using STA-FTIR (Fig. 2). The data show percentage mass ("% weight") and heat flow, and evolved gas analysis as FTIR RMS intensity ("$FTIR_{RMS}$"), which is the mean FTIR absorbance intensity over the entire frequency range measured (4000 – 500 cm^{-1}). The temperature range 30 - 400 °C was scanned at a rate of 10 °C min^{-1}.

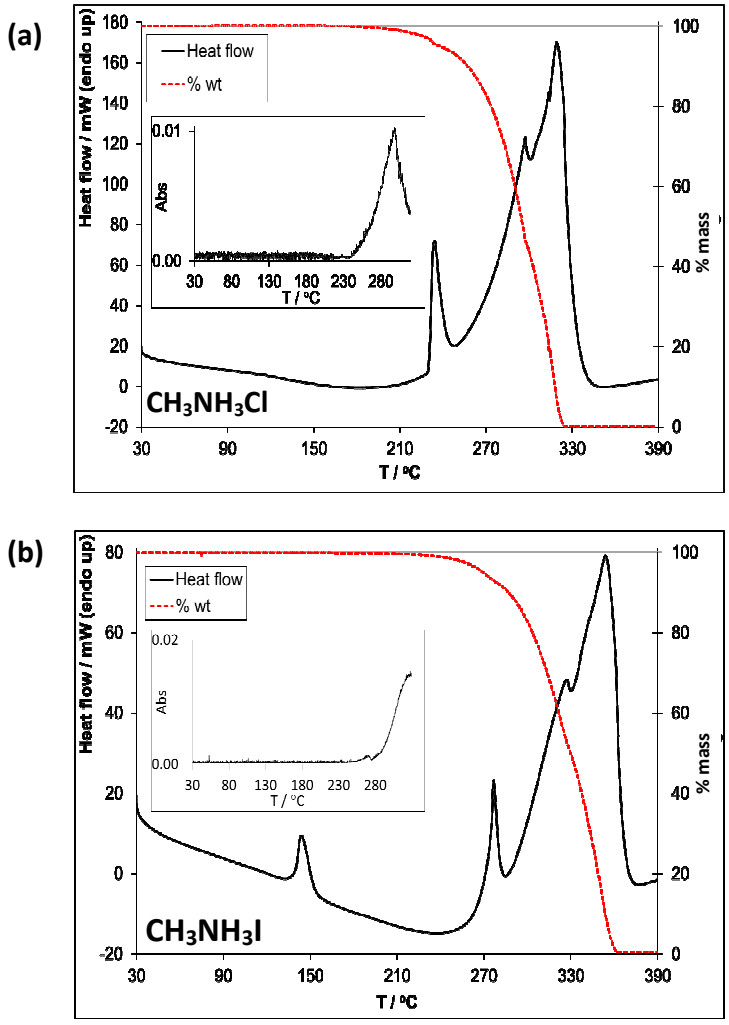

Figure 2: STA-FTIR data measured at 10 °Cmin^{-1} under N_2 for (a) CH_3NH_3Cl and (b) CH_3NH_3I. Insets are $FTIR_{RMS}$ intensity profiles measured until mass = 0 %. Heat flow curves are not baseline-corrected so only show main thermal events.

The mass loss data (dashed lines) show that loss begins around 190 °C for CH_3NH_3Cl and around 210 °C for CH_3NH_3I. The DSC data (solid lines) for CH_3NH_3Cl show a sharp endotherm at around 230 °C; correspondingly, there is a small step in the mass loss. Around the same temperature, the gas evolved (as shown by the $FTIR_{RMS}$ intensity) begins to increase. Prior to this there is no evidence for any gas evolution and certainly not at the common annealing temperature of 100 °C (ESI Fig. 2).

By comparison, the heat flow data for CH_3NH_3I (Fig. 2b) exhibit an endotherms at *ca.* 140 °C. This is well-documented and corresponds to an $\alpha^1 \rightarrow \varepsilon$ solid-solid phase transition, producing a metastable, 'pre-melting' state without any mass loss.[22,29] The data then show a sharp endotherm at *ca.* 275 °C, which is accompanied by a small step in the mass loss curve as for CH_3NH_3Cl. For CH_3NH_3I, no gas evolution is observed until *ca.* 240 °C when the $FTIR_{RMS}$ intensity plot shows a small signal before gas evolution increases significantly at *ca.* 275 °C.

The FTIR spectra of the evolved gas at 225 °C start to show broad peaks at *ca.* 750 and *ca.* 3000 cm^{-1} for CH_3NH_3Cl, and some structure can be discerned from the noise between *ca.* 1750 and *ca.* 500 cm^{-1} for CH_3NH_3I; these features become a little more distinct at *ca.* 247 °C. For both salts, these peaks are fully resolved by 265 °C and further peaks can also be seen (Fig. 3). The spectrum for CH_3NH_3Cl (Fig. 3a) shows peaks for $CH_3NH_{2(g)}$ and $HCl_{(g),}$[35] although the R-branch of the HCl spectrum *ca.* 3000 cm^{-1} is relatively more intense than the P-branch owing to overlap with the ν_2 mode (CH_3 stretch)[36] of methylamine. This suggests that CH_3NH_3Cl decomposes to CH_3NH_2 and HCl as reported previously.[31,32] In contrast, the spectrum of CH_3NH_3I (Fig. 3b) shows no evidence of $HI_{(g)}$ *ca.* 2229 cm^{-1} or CH_3NH_2. Instead, peaks characteristic of ammonia and methyl iodide are observed.[35] As there is no evidence of CH_3Cl[35] or ammonia in Fig. 3a, this suggests different decomposition routes for the CH_3NH_3Cl and CH_3NH_3I salts. It has been predicted that primary alkylammonium halides decompose to form CH_3NH_2 + HX;[32] however, these data show that, while this holds true for CH_3NH_3Cl, this is not the case for CH_3NH_3I.

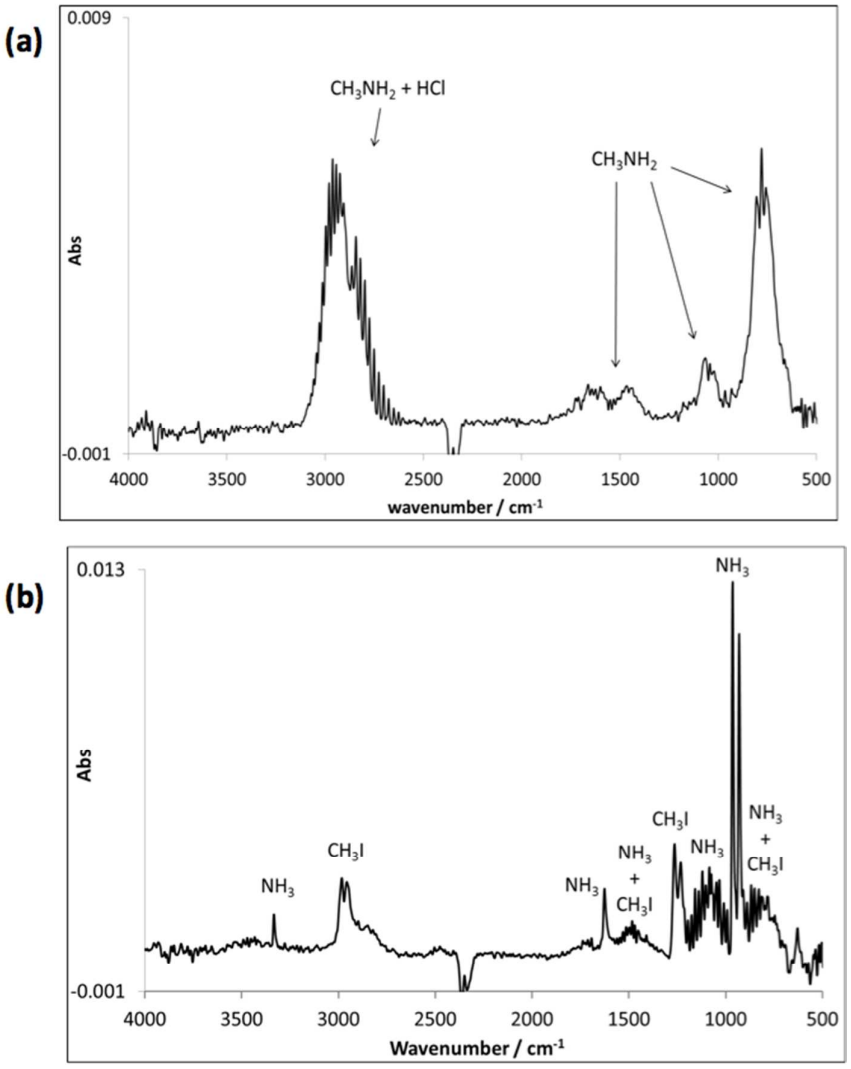

Figure 3: FTIR spectra of gases evolved from (a) CH_3NH_3Cl and (b) CH_3NH_3I at *ca.* 265 °C

Overall, these data for the pure salts suggest that, if CH_3NH_3Cl were formed upon processing at 100 °C as suggested previously,[13] then there is no sublimation of either CH_3NH_3Cl or CH_3NH_3I.

Solutions of $CH_3NH_3PbI_{3-x}Cl_x$ and $CH_3NH_3PbI_3$ (40 wt. % in DMF) were then studied isothermally using STA-FTIR at 100 °C for 80 min (Fig. 4). FTIR spectra of the evolved gases (Fig. 4a) show that only DMF is evolved from either precursor solution during annealing at 100 °C. Temporal changes in the intensity of the carbonyl band stretch of DMF (*ca.* 1720 cm^{-1}; "$FTIR_{1720}$") show an increase to a maximum after *ca.* 7 min, which decreases rapidly to between 12 and 18 min (Fig. 4b). This is followed by a much slower rate of DMF evolution, which occurs up to *ca.* 60 min, after which time the signal disappears. This suggests complete solvent loss has been achieved by 80 min.

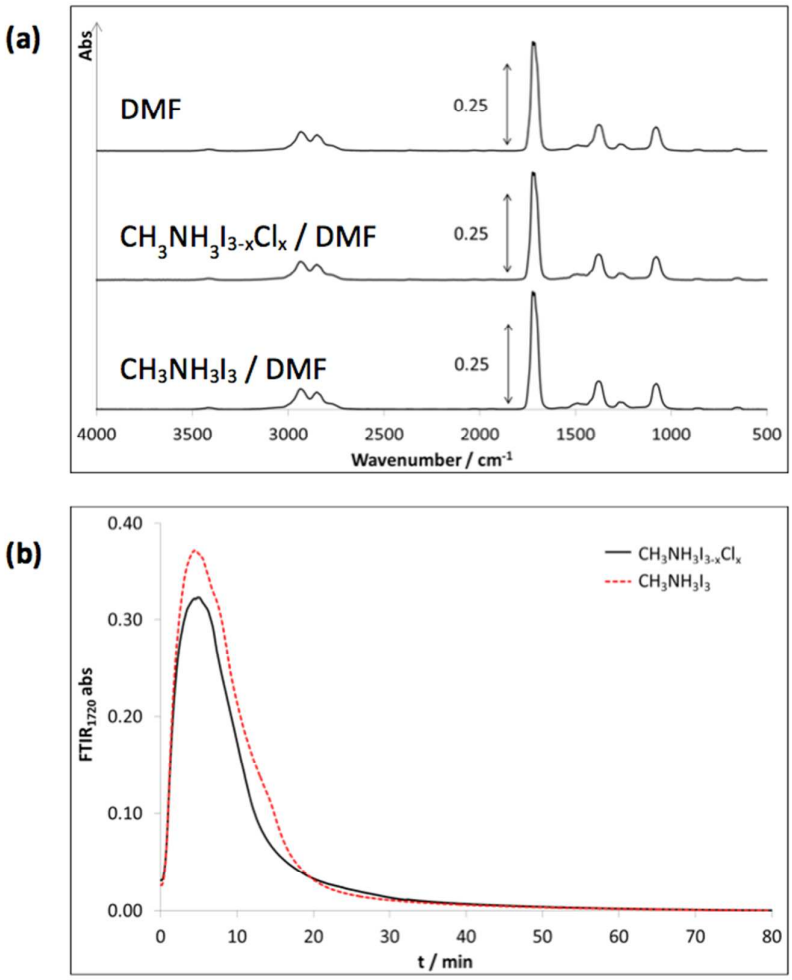

Figure 4: (a) FTIR spectra of evolved gas from neat DMF, and $CH_3NH_3I_{3-x}Cl_x$ and $CH_3NH_3I_3$ (40 wt. %) in DMF, held isothermally at 100 °C. $CH_3NH_3I_{3-x}Cl_x$ and $CH_3NH_3I_3$ spectra were taken at 5 min. (b) $FTIR_{1720}$ band profiles for $CH_3NH_3I_{3-x}Cl_x$ and $CH_3NH_3I_3$

To test whether solvent has been completely removed from the materials after 80 min, annealed samples were analysed by STA-FTIR from 30 – 200 °C. The evolved gas FTIR data are shown in Fig. 5. These data indicate that, for both $CH_3NH_3PbI_{3-x}Cl_x$ and $CH_3NH_3PbI_3$, $DMF_{(g)}$ is still evolved even after annealing for 80 min at 100 °C. Increasing $DMF_{(g)}$ is liberated as the sample temperature is increased from 20 to 200 °C, whilst there is no evidence of any other gaseous species. These suggest that Cl^- is not lost from $CH_3NH_3PbI_{3-x}Cl_x$ during annealing under these conditions. It is also worth noting that the higher intensity solvent signal seen for the $CH_3NH_3PbI_3$ compared with the $CH_3NH_3PbI_{3-x}Cl_x$ (Fig. 5b) is attributable to a larger amount of sample for $CH_3NH_3PbI_3$ rather than greater retention of, or affinity for, the solvent. Upon heating the samples to 230 °C (ESI Fig. 3), although $DMF_{(g)}$ is still observed, other species begin to appear. $CH_3NH_3PbI_{3-x}Cl_x$ begins to break down to $CH_3NH_{2(g)}$ and $HCl_{(g)}$, suggesting that the decomposition mechanism of this material is similar to that of CH_3NH_3Cl. In comparison, at this temperature $CH_3NH_3PbI_3$ still shows dominant $DMF_{(g)}$ but weaker features attributable to $NH_{3(g)}$ (*ca.* 1000 cm^{-1}) begin to appear, suggesting some decomposition following a mechanism similar to that of CH_3NH_3I.

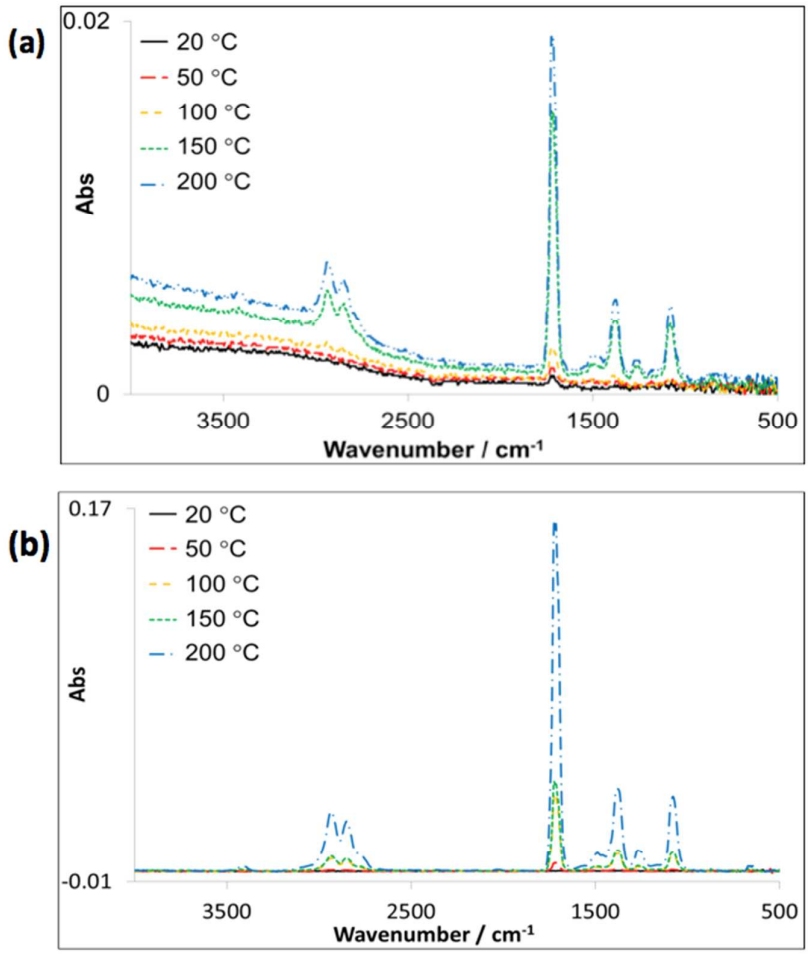

Figure 5: Post-anneal evolved gas FTIR spectra of perovskites previously 'annealed' at 100 °C. Spectra acquired at sample temperatures 20, 50, 100, 150 and 200 °C. (a) $CH_3NH_3I_{3-x}Cl_x$, (b) $CH_3NH_3I_3$

The solvent retention is not surprising, as it is known that materials produced from heated solution deposition can retain solvent for years;[37] however, the amount of solvent retained given different preparation methods, and the impact this has on material performance and stability, warrants further investigation. To probe these effects, and to minimise solvent interference, $CH_3NH_3PbI_{3-x}Cl_x$ was subjected to pre-drying or 'alternative annealing' methods prior to STA-FTIR. Firstly, as a control and to compare to previous data,[12] $CH_3NH_3I_{3-x}Cl_x$ precursor solution (40 wt. % in DMF) was left to dry slowly at 30 °C under N_2 *in-situ* to remove as much superficial solvent as possible prior to STA-FTIR analysis (Fig. 6). During the 30 °C 'pre-drying' step, the dominant evolved gas species observed by FTIR was DMF (ESI Fig. 4); DMF evolution was seen to decrease gradually until levelling at *ca.* 8 h, which correlates with mass loss data (Fig. 6a, inset). Close examination of the FTIR data (ESI Fig. 4) shows no DMF signal after *ca.* 11 h, suggesting all liquid DMF has evaporated.

Following the 'pre-drying' step, gas evolution from the $CH_3NH_3PbI_{3-x}Cl_x$ at 100 °C was analysed by STA-FTIR for 90 min using the intensity of the 1720 cm^{-1} DMF carbonyl peak (Fig. 6b).

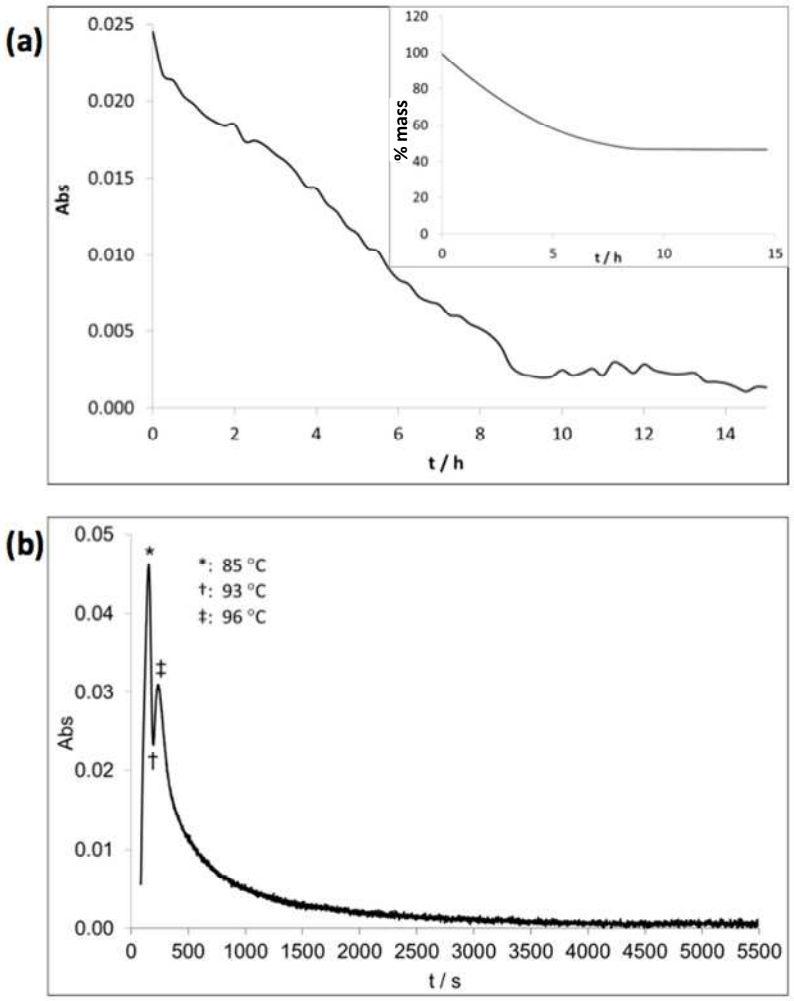

Figure 6: (a) Intensity of evolved gas $FTIR_{RMS}$ peak and (inset) % mass loss for $CH_3NH_3PbI_{3-x}Cl_x$ undergoing solvent loss at 30 °C under N_2. (b) $FTIR_{1720}$ intensity of evolved gas from 'pre-dried' $CH_3NH_3PbI_{3-x}Cl_x$ undergoing annealing at 100 °C under N_2.

The data in Fig. 6b show very rapid increase in DMF release in the first 100 s as the sample reaches 100 °C. The rate of $DMF_{(g)}$ evolution then decreases and becomes increasingly slow up to *ca.* 4000 s. The associated FTIR spectra (ESI Fig. 5) confirm the evolved gas is DMF, although some CO_2 is also observed. The CO_2 signal remains constant over the time period 500 – 5500 s and could be attributable to release of dissolved CO_2. In the presence of water, DMF is also known to undergo gradual degradation to formic acid and dimethylamine[38] and thermal decomposition of the former species could lead to the liberation of CO_2.

Following pre-drying at 30 °C (900 min) and subsequent annealing at 100 °C (90 min) (Fig. 6), the temperature of this sample of $CH_3NH_3PbI_{3-x}Cl_x$ was ramped to 250 °C at 10 °Cmin^{-1} and held isothermally. The intensity of the $FTIR_{1720}$ band (Fig. 7) varies considerably over the temperature range shown, with a number of sharp peaks. This profile is reproducible, as illustrated in ESI Fig. 6d. The associated FTIR spectra confirm that DMF dominates the evolved gas (ESI Fig. 6a and b) until 236 °C, when additional peaks for HCl are seen at *ca.* 3000 cm^{-1} (ESI Fig. 6b) indicating initial decomposition of the material. ESI Fig. 6c shows a spectrum at 240 °C, which was taken at the start of a further isothermal step, and shows very little DMF but significant HCl and CH_3NH_2 as decomposition products. These data show that, despite pre-drying at 30 °C and annealing at 100 °C, some Cl^- remains in the film because some HCl is evolved during sample

decomposition.

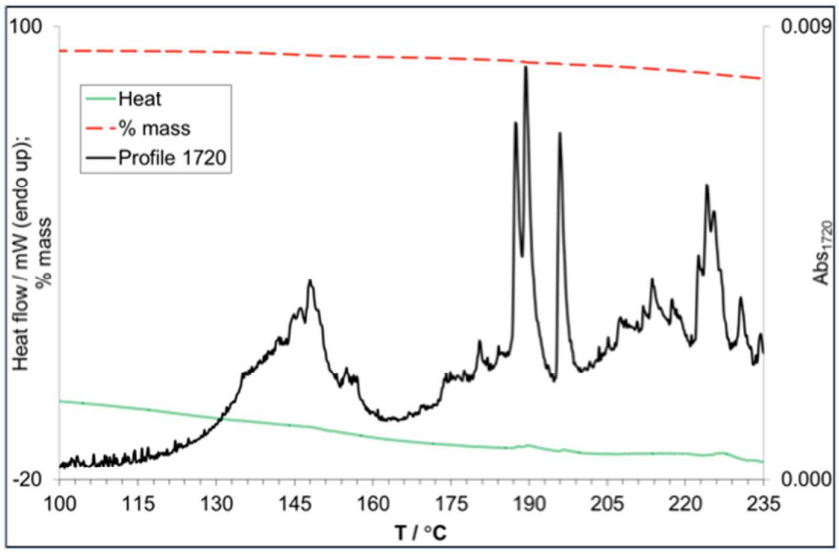

Figure 7: DTA-FTIR analysis over the temperature range 100 – 250 °C for sample of $CH_3NH_3I_{3-x}Cl_x$ that had been subjected to 30 °C for 900 minutes and 100 °C for 90 minutes

The data in Fig. 7 suggest that the DMF loss is associated with thermally-induced events that liberate DMF that is part of the $CH_3NH_3PbI_{3-x}Cl_x$ lattice rather than simple evaporation, which would result in a much more consistent solvent loss. This is supported by endothermic peaks in the heat flow at *ca.* 145, 190 and 230 °C, which coincide with further DMF loss. Resolving these DMF loss features also highlights the importance of slow, pre-drying the samples prior to analysis, as this seems to eliminate DMF that is easily removed, and which would otherwise swamp these signals.

To study DMF loss from $CH_3NH_3PbI_{3-x}Cl_x$ under conditions closer to those used in perovskite device manufacture, mixed halide precursor solutions (40 wt. % in DMF) were subjected to three different annealing conditions: 30 °C for 900 min, 100 °C for 10 min and 100 °C for 80 min. After each treatment, the samples had apparently reached 40 % of the initial mass and the heat flow and DMF evolution had stabilised. After annealing, each sample was further analysed by STA-FTIR (30 – 200 °C at 10 °Cmin^{-1}) (Fig. 8). The data show that, as might be expected, there is still residual DMF within the samples after each annealing procedure (ESI Fig. 7). In each case, DMF is evolved from 30 °C onwards (Fig. 8) with maximum gas evolution between *ca.* 130 and *ca.* 190 °C.

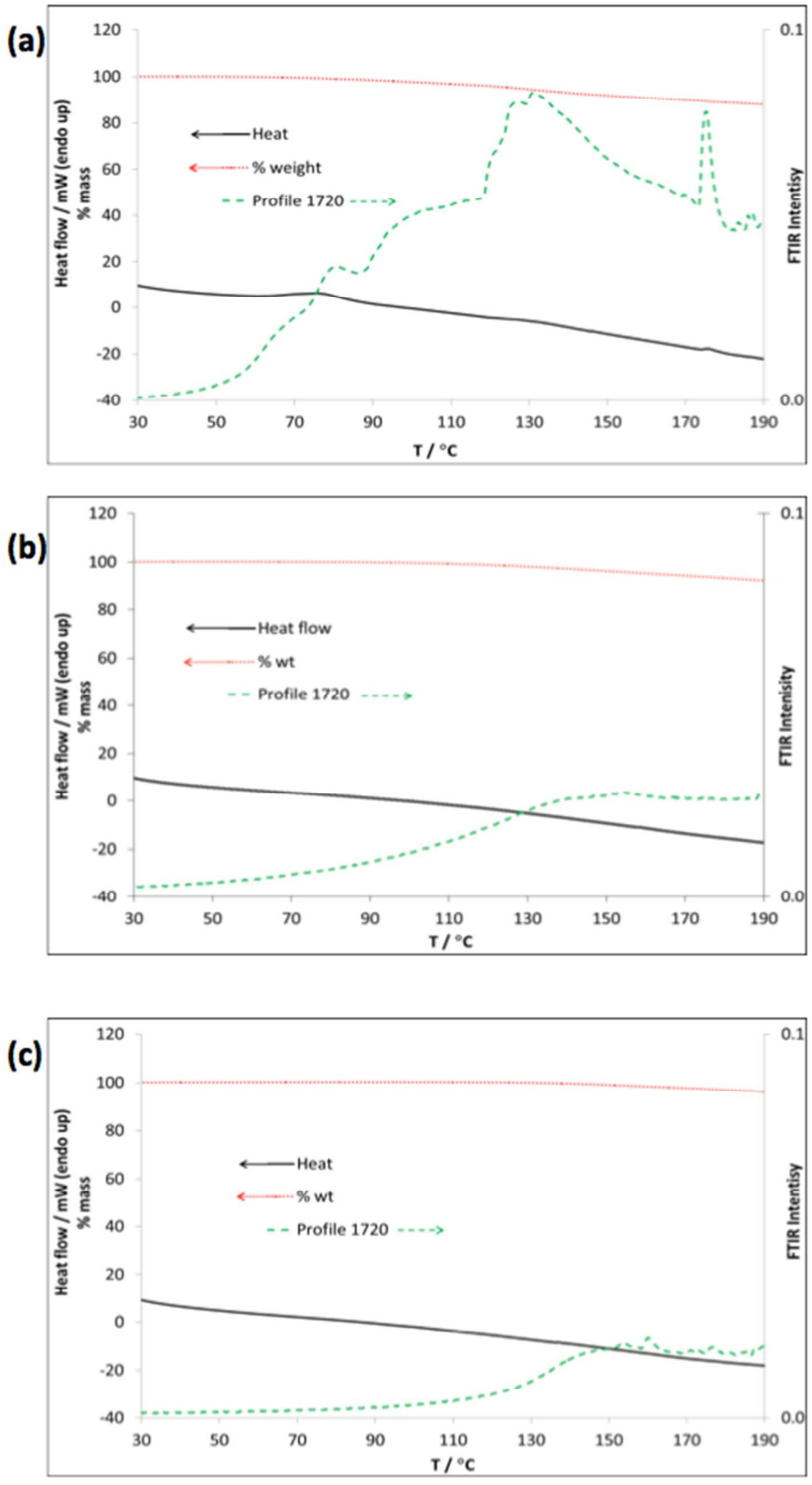

Figure 8: Post- anneal STA and $FTIR_{1720}$ profiles of $CH_3NH_3I_{3-x}Cl_x$ annealed at (a) 30 °C for 900 min; post-cure scan; (b) 100 °C for 10 min; (c) 100 °C for 80 min.

The maximum intensity correlates broadly with the amount of solvent present. The sample 'annealed' at 30 °C (Fig. 8a) shows the largest DMF evolution based on $FTIR_{1720}$ intensity, while the sample annealed at 100 °C for 80 min (Fig. 8c) shows the smallest, as might be expected. The DMF evolution, $FTIR_{1720}$ profiles for both

samples that were annealed at 100 °C (Fig. 8b and c) lack the fine structure seen for the sample that was pre-dried prior to annealing (Fig. 7), probably owing to concurrent release of bound and 'free' solvent. Examining the scale of these data, it can also be seen that the overall intensity of the $FTIR_{1720}$ signal in Fig. 7, omitting the spikes, is almost an order of magnitude smaller than the signals in Fig. 8b and c, further indicating the presence of 'free' solvent. It should be noted that by re-scaling these data as shown in ESI Fig. 6d, spiking becomes apparent. The STA data in Fig. 8b and c show steadily decreasing signals with little evidence of specific thermal events.

The sample that had been 'annealed' at 30 °C shows distinct features both in the $FTIR_{1720}$ signal with peaks at *ca.* 75, 110, 135 and 175 °C, suggesting that progressively strongly bound DMF is being released with increasing temperature. The peaks correspond to small endothermic deflections in heat flow, indicative of solvent release following increasingly energetic processes. The differences between the samples annealed at the different temperatures could be attributable to different solvent loss mechanisms. Processing at the higher temperature of 100 °C could give rise to complete solvent loss from the surface of the material; however, solvent could remain trapped within the crystal structure. Given the size and polarity of DMF, it is conceivable that it would associate with the perovskite's lattice structure.

3.2. Alternative method of solvent removal: desiccant

It is evident that annealing a sample at 30 or 100 °C does not completely remove DMF, and even pre-drying at 30 °C followed by annealing at 100 °C results in significant solvent retention. It also appears that the higher temperature annealing alters the crystal lattice. To avoid this, silica gel desiccant was used to air-dry (RT) $CH_3NH_3PbI_{3-x}Cl_x$ (40 wt. % in DMF). STA-FTIR data for a sample dried (verified by observation) in this method for 3 days are shown in Fig. 9.

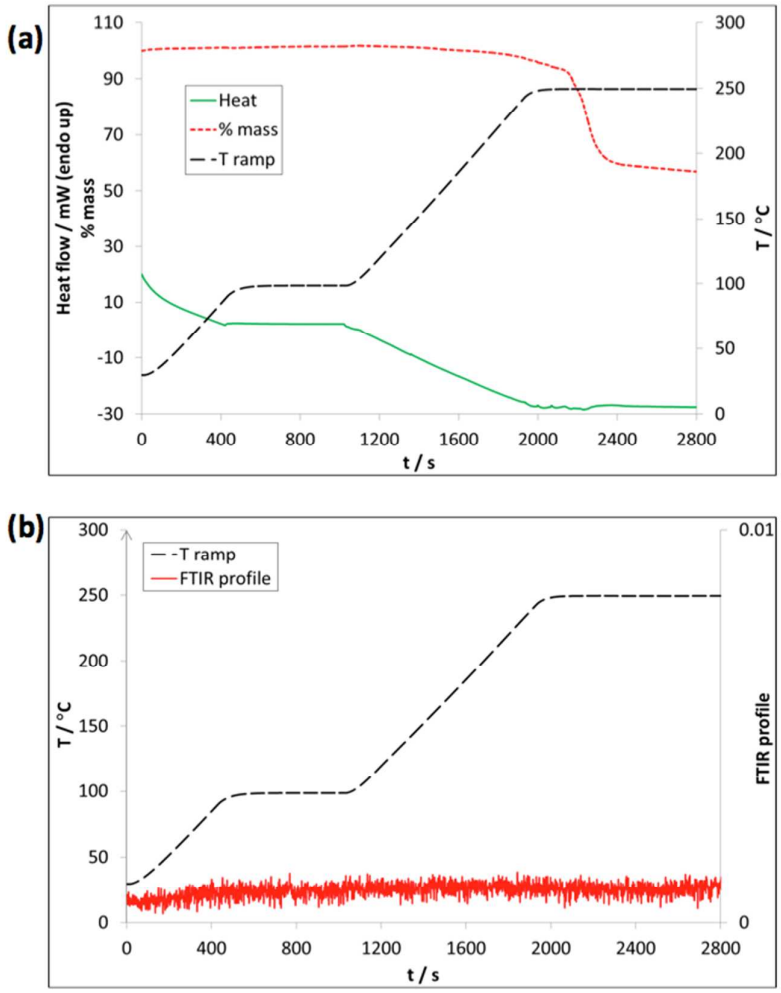

Figure 9: STA-FTIR data for a sample of $CH_3NH_3I_{3-x}Cl_x$ 40 wt. % in DMF dried at room temperature using silica gel desiccant. (a) temperature ramp and STA profiles; (b) temperature ramp and $FTIR_{RMS}$ intensity profile

The data show that there is negligible DMF remaining in the sample after drying using silica gel. There is no change in heat flow (aside from those associated with temperature ramping), no significant mass loss until *ca.* 250 °C, and no increase in $FTIR_{RMS}$ intensity (Fig. 9b). Corresponding FTIR spectra (ESI Fig. 8) show no signals until 249 °C, where a very small peak appears around 1720 cm^{-1}. Thus, desiccated samples differ significantly from thermally dried material by not exhibiting DMF release or any by-products of decomposition. These data suggest that desiccants may be a viable way of enabling facile solvent-free material studies, which may be important for enhancing device lifetimes.

3.5. Structural Information by DSC: Annealed $CH_3NH_3I_{3-x}Cl_x$ and $CH_3NH_3I_3$

There has been speculation that, during the annealing phase of the $CH_3NH_3I_{3-x}Cl_x$ perovskite preparation, Cl^- is lost and the resulting film is actually $CH_3NH_3PbI_3$;[30] therefore, DSC analysis from 20 – 120 °C was performed on a sample of each of $CH_3NH_3I_{3-x}Cl_x$ and $CH_3NH_3I_3$, which had been prepared by annealing a sample (40 wt. % in DMF) *in situ* at 100 °C under N_2 as previously described (Fig. 10).

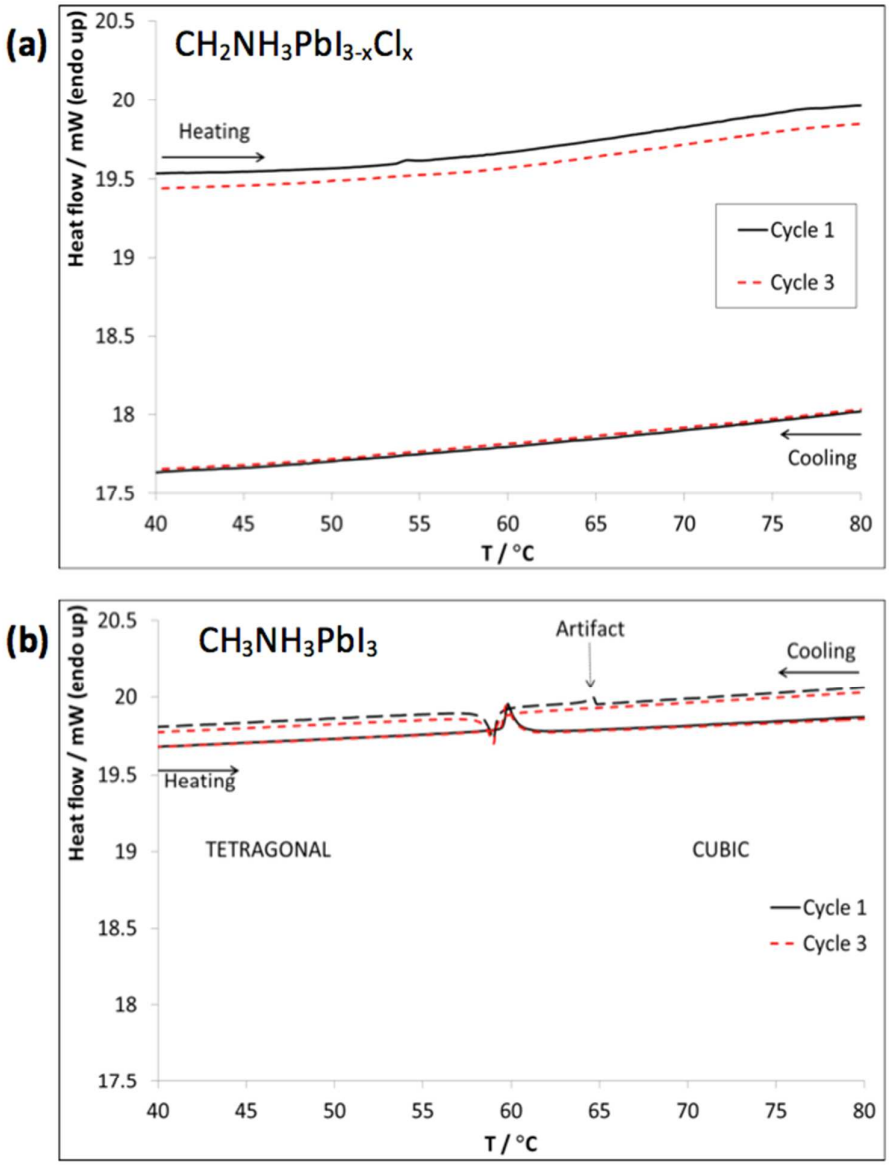

Figure 10: DSC of (a) $CH_3NH_3PbI_{3-x}Cl_x$ and (b) $CH_3NH_3PbI_3$ after pre-annealing *in-situ* at 100 °C

The DSC of the $CH_3NH_3PbI_3$ (Fig. 10b) shows a sharp endotherm *ca.* 60 °C, which corresponds to the tetragonal-cubic phase transition.[39] The transition back to the tetragonal phase is apparent on cooling showing it to be a reversible process, and the whole cycle is repeatable. The feature seen *ca.* 65 °C on the cooling scan of cycle 1 (Fig. 10b) is almost certainly an artefact, possibly caused by movement of the sample, and was not seen in subsequent scans or repeat tests. In comparison, the $CH_3NH_3PbI_{3-x}Cl_x$ sample (Fig. 10a) shows no phase transition, suggesting that the final material prepared from the mixed halide precursor solution is not simply $CH_3NH_3PbI_3$. The scans also show different general characteristics, indicative of different thermal properties. For example, although the nature of the test prevented exact sample masses being measured, comparable amounts of sample were used, so the qualitative differences in heat flow between the two samples indicates differences in their heat capacities. These DSC results alone might indicate that a different form of $CH_2NH_3PbI_3$, which does not undergo a thermally-induced transition to the tetragonal or cubic phase, is present; however, when coupled with the observation that decomposition of

material prepared from $CH_3NH_3I_{3-x}Cl_x$ evolves HCl, the argument that Cl^- is still present in these films is strengthened.

4 Conclusions

Thermal and evolved gas analyses show that, whilst heat treatment does not remove DMF solvent from methyl ammonium lead halides, desiccation using silica gel achieves almost total solvent removal at ambient temperature and pressure. This is important because the role of residual solvent in the perovskite lattice during PV operation is not yet clear, but it is possible that this may influence device lifetimes. Our data also show no evidence for methyl ammonium halide being lost from the lattice until temperatures over 150°C, *i.e.* well above typical processing temperatures used for perovskite PV devices. On the other hand, HCl is regularly observed for $CH_3NH_3PbI_2Cl$ at higher temperatures, implying that some Cl must remain within the mixed halide film of this material.

5 Acknowledgements

This work was supported by the Engineering and Physical Sciences Research Council and the Technology Strategy Board through the SPECIFIC Innovation and Knowledge Centre (grant numbers EP/ I019278/1, EP/K000292/1, EP/L010372/1) and the Welsh Government for support to the Sêr Solar programme. We would like to acknowledge funding by the European Social Fund (ESF) through the European Union's Convergence programme administered by the Welsh Government. We also acknowledge invaluable help provided by Olivier Savard and the rest of the team at Perkin Elmer, Seer Green, Bucks., UK.

6 References

1. A. Kojima, K. Teshima, Y. Shirai, and T. Miyasaka, *J. Am. Chem. Soc. Commun.*, 2009, **131**, 6050–1.

2. H.-S. Kim, C.-R. Lee, J.-H. Im, K.-B. Lee, T. Moehl, A. Marchioro, S.-J. Moon, R. Humphry-Baker, J.-H. Yum, J. E. Moser, M. Grätzel, and N.-G. Park, *Sci. Rep.*, 2012, **2**, 591.

3. M. M. Lee, J. Teuscher, T. Miyasaka, T. N. Murakami, and H. J. Snaith, *Science*, 2012, **338**, 643–7.

4. L. Etgar, P. Gao, Z. Xue, Q. Peng, A. K. Chandiran, and B. Liu, *J. Am. Chem. Soc.*, 2012, 3–6.

5. J. M. Ball, M. M. Lee, A. Hey, and H. J. Snaith, *Energy Environ. Sci.*, 2013, 1739–1743.

6. J. Burschka, N. Pellet, S.-J. Moon, R. Humphry-Baker, P. Gao, M. K. Nazeeruddin, and M. Grätzel, *Nature*, 2013, **499**, 316–9.

7. M. J. Carnie, C. Charbonnaeu, M. L. Davies, B. C. O'Regan, D. A. Worsley, T. M. Watson, and C. Charbonneau, *J. Mater. Chem. A*, 2014, **2**, 17077–17084.

8. M. J. Carnie, C. Charbonneau, M. L. Davies, J. Troughton, T. M. Watson, K. Wojciechowski, H. Snaith, and D. A. Worsley, *Chem. Commun.*, 2013, **49**, 7893–5.

9. David B. Mitzi (IBM T. J. Watson Research Center), *Progress in Inorganic Chemistry, Volume 48*, Wiley Online Library, NY, 1999.

10. D. B. Mitzi, C. A. Feild, Z. Schlesinger, and R. B. Laibowitz, *J. Solid State Chem.*, 1995, **114**, 159–163.

11. A. Barrows, A. Pearson, C. Kwak, A. Dunbar, A. Buckley, and D. Lidzey, *Energy Environ. Sci.*, 2014, **7**, 2944–2950.

12. G. E. Eperon, V. M. Burlakov, P. Docampo, A. Goriely, and H. J. Snaith, *Adv. Funct. Mater.*, 2013, **24**, 151–157.

13. A. Dualeh, N. Tétreault, T. Moehl, P. Gao, M. K. Nazeeruddin, and M. Grätzel, *Adv. Funct. Mater.*, 2014, **24**, 3250–3258.

14. V. M. Burlakov, G. E. Eperon, H. J. Snaith, S. J. Chapman, and A. Goriely, *Appl. Phys. Lett.*, 2014, **104**, 091602–1 – 091602–5.

15. S. Y. Dou, L. T. Yan, Y. C. Liu, G. Du, and P. Zhou, *J. Mater. Sci. Mater. Electron.*, 2013, **24**, 4862–4867.

16. J. Jeng, Y. Chiang, M. Lee, T. Guo, P. Chen, and T. Wen, *SPIE Newsroom*, 2013, August 8.

17. I. Chung, B. Lee, J. He, R. P. H. Chang, and M. G. Kanatzidis, *Nature*, 2012, **485**, 486–9.

18. T. Supasai, N. Rujisamphan, K. Ullrich, a. Chemseddine, and T. Dittrich, *Appl. Phys. Lett.*, 2013, **103**, 183906.

19. R. H. Mitchell, in *Perovskites: Modern and Ancient*, Almaz Press Inc., Ontario, 2002, pp. 181–194.

20. T. Baikie, Y. Fang, J. M. Kadro, M. Schreyer, F. Wei, S. G. Mhaisalkar, M. Graetzel, and T. J. White, *J. Mater. Chem. A*, 2013, **1**, 5628.

21. Y. Kawamura, H. Mashiyama, K. Hasebe, and K. Kawamura, Y., Mashiyama, H. and Haseby, *J. Phys. Soc. Japan*, 2002, **71**, 1694–1697.

22. O. Yamamuro, T. Matsuo, H. Suga, W. I. F. David, R. M. Ibberson, and A. J. Leadbetter, *Acta Crystallogr. Sect. B Struct. Sci.*, 1992, **B48**, 329–336.

23. O. Yamamura, N. Onoda-Yamamuro, H. Suga, T. Kamiyama, T. Ishigaki, and H. Asano, *J. Phys. Chem. Solids*, 1994, **55**, 383–389.

24. R. D. Waldron, *J. Chem. Phys.*, 1953, **21**, 734–741.

25. C. Theoret, A. and Sandorfy, *Spectrochim. Acta*, 1967, **23A**, 519–542.

26. H.Ishida, R.Ikeda, and D.Nakamura, *J. Phys. Chem.*, 1982, **86**, 1003–1008.

27. C. Cabana, A. and Sandorfy, *Spectrochim. Acta*, 1962, **18**, 843–861.

28. C. W. Aston, J.G. and Ziemer, *J. Am. Chem. Soc.*, 1946, **68**, 1405–1413.

29. D. Ishida, H., Ikeda, R. and Nakamura, *Phys. Stat. Sol.*, 1982, **70**, K151–K154.

30. A. Dualeh, P. Gao, S. Il Seok, M. K. Nazeeruddin, and M. Grätzel, *Chem. Mater.*, 2014, 140815172547009.

31. M. Sawicka, P. Storoniak, J. Błazejowski, and J. Rak, *J. Phys. Chem. A*, 2006, **110**, 5066–74.

32. M. Sawicka, P. Storoniak, P. Skurski, J. Błażejowski, and J. Rak, *Chem. Phys.*, 2006, **324**, 425–437.

33. S. S. Joshi, T. M. Aminabhavi, R. H. Balundgi, and S. S. Shukla, *J. Chem. Eng. Data*, 1990, **35**.

34. D.R. Lide, *CRC Handbook of Chemistry and Physics 88th Edition*, CRC Press, Taylor & Francis, Boca Raton, FL.

35. 20899. Eds. P.J. Linstrom and W.G. Mallard, National Institute of Standards and Technology, Gaithersburg MD, .

36. University of Washington, *Virtual Planet. Lab. http//vpl.astro.washington.edu/spectra/frontpage. Retrieved 31st August 2014*.

37. D. A. W. Zeno W. Wicks, Jr., Frank N. Jones, S. Peter Pappas, *Organic Coatings: Science and Technology*, Wiley, 3rd edn., 2007.

38. J. Juillard, *Pure Appl. Chem.*, 1977, **49**, 885–892.

39. K. Kawamura, Y., Mashiyama, H. and Haseby, *J. Phys. Soc. Japan*, 2002, **71**, 1694–1697.

Graphical Abstract: Perovskite Processing for Photovoltaics: a Spectro-Thermal Evaluation

A.E. Williams,[a] P.J. Holliman,[b] M.J. Carnie,[a] M.L. Davies,[a] D. A. Worsley,[a] T.M. Watson[a]

[a] SPECIFIC, College of Engineering Swansea University, Baglan Bay Innovation and Knowledge Centre, Port Talbot SA12 7AZ (UK)
[b] School of Chemistry, Bangor University, Bangor, Gwynedd LL57 2UW (UK)

A real-time analysis by STA-FTIR of changes occurring and volatiles evolved during processing of perovskites for PV technology. Solvent retention, presence of chemical species and decomposition of materials can be evaluated to gain insight into material composition.